




A Modified Fifth Order Finite Difference Hermite WENO Scheme for Hyperbolic Conservation Laws

Zhuang Zhao¹ · Yong-Tao Zhang² · Jianxian Qiu³ 

Received: 28 June 2020 / Revised: 6 September 2020 / Accepted: 12 October 2020
© Springer Science+Business Media, LLC, part of Springer Nature 2020

Abstract

In this paper, we develop a modified fifth order accuracy finite difference Hermite WENO (HWENO) scheme for solving hyperbolic conservation laws. The main idea is that we first modify the derivatives of the solution by Hermite WENO interpolations, then we discretize the original and derivative equations in the spatial directions by the same approximation polynomials. Comparing with the original finite difference HWENO scheme of Liu and Qiu (J Sci Comput 63:548–572, 2015), one of the advantages is that the modified HWENO scheme is more robust than the original one since we do not need to use the additional positivity-preserving flux limiter methodology, and larger CFL number can be applied. Another advantage is that higher order numerical accuracy than the original scheme can be achieved for two-dimensional problems under the condition of using the same approximation stencil and information. Furthermore, the modified scheme preserves the nice property of compactness shared by HWENO schemes, i.e., only immediate neighbor information is needed in the reconstruction, and it has smaller numerical errors and higher resolution than the classical fifth order finite difference WENO scheme of Jiang and Shu (J Comput Phys 126:202–228, 1996). Various benchmark numerical tests of both one-dimensional and two-dimensional problems are presented to illustrate the numerical accuracy, high resolution and robustness of the proposed novel HWENO scheme.

Keywords Hermite WENO scheme · Finite difference method · Hyperbolic conservation laws · Modification for derivative · Hermite interpolation

Mathematics Subject Classification 65M60 · 35L65

Z. Zhao and J. Qiu were supported partly by Science Challenge Project (China), No. TZ 2016002 and National Natural Science Foundation-Joint Fund (China) Grant U1630247. Y.-T. Zhang was partially supported by NSF Grant DMS-1620108 (USA). This work was carried out while Z. Zhao was visiting the Department of Applied and Computational Mathematics and Statistics, the University of Notre Dame under the support by the China Scholarship Council (CSC: 201906310075).

Extended author information available on the last page of the article

1 Introduction

In this paper, we propose a modified fifth order Hermite weighted essentially non-oscillatory (HWENO) scheme in the finite difference framework for one-dimensional and two-dimensional problems. HWENO scheme was derived from essentially non-oscillatory (ENO) and weighted essentially non-oscillatory (WENO) schemes, and they have been widely applied for solving nonlinear hyperbolic conservation laws in recent decades. As it is known, the solution of the nonlinear hyperbolic conservation laws often contains shock, contact discontinuities and sophisticated smooth structures, simultaneously. Hence the development of high order numerical methods for solving them is challenging. The pioneering work by Harten et al. [7,8] introduced the finite volume ENO schemes, which used a weaker version of the total variation diminishing (TVD) criterion [6]. Then, Shu and Osher [23,24] proposed a class of finite difference ENO schemes for efficiently solving multidimensional problems. ENO schemes select approximation stencil adaptively based on the local smoothness of candidate stencils, so their numerical accuracy is determined by one of the candidate stencils. To improve the accuracy of ENO schemes, in 1994 Liu, Osher and Chan [14] firstly constructed a third-order finite volume WENO scheme based on ENO schemes, in which they employed a nonlinear convex combination of all candidate stencils to achieve higher order accuracy in smooth regions. In 1996, Jiang and Shu [11] proposed the third and fifth order finite difference WENO schemes for multidimensional problems, where they gave a general framework to design the smoothness indicators and nonlinear weights. Ever since then, WENO schemes have been further developed and studied extensively, see e.g. [3,10,12,13,21,29,30,35].

On the other hand, a higher order accuracy WENO scheme needs to use a wide stencil for the reconstruction. That leads to some difficulties in the application of the method. In order to balance the compactness and numerical accuracy of WENO schemes, Qiu and Shu [19,20] developed a new finite volume scheme based on WENO schemes via dealing with both the solution and its derivatives. It is termed as Hermite WENO (HWENO) scheme. In the original HWENO schemes, different polynomials are used in the spatial discretizations of the original partial differential equation (PDE) and the equations satisfied by derivatives of the solution. The schemes are compact, but there are some difficulties when they are applied in simulating some benchmark problems such as the double Mach and the forward step problems. This issue was resolved by Zhu and Qiu in [34], where a new procedure to reconstruct the derivative terms was designed. Later, Liu and Qiu [15,16] proposed the fifth order finite difference HWENO scheme, in which an additional positivity-preserving flux limiter methodology [1,9] has to be used to ensure the robustness of the method. As a continuation of the work, Zahran and Abdalla [28] extended the fifth order finite difference HWENO scheme [15] to higher order accuracy, and Ma and Wu [18] developed a compact HWENO scheme, in which they solved the first derivative values of the solution by the compact difference method, while Cai et al. [2] employed the strong stability preserving (SSP) multi-step temporal discretization procedure for the HWENO schemes [19,34]. The unknown variables solved in these finite volume and finite difference HWENO schemes [1,2,15,16,18–20,25,28,34] are the solution of the PDE and its derivatives. Another type of finite volume HWENO schemes [17,26,31–33] solved equations satisfied by the solution of the PDE and its first order moments. The concept of moments comes from the discontinuous Galerkin (DG) method [4], and the $P_N P_M$ method by Dumbser et al. in [5] where a general and unified framework to define the numerical scheme extended by DG method was provided. All of these HWENO schemes [1,2,15–20,25,26,28,33,34] used different stencils and approximation polynomials in the

spatial discretizations of the original PDE and the equations satisfied by derivatives or the first order moments of the solution. The derivatives or the first order moments of the solution were used straightforwardly in the schemes. They could be quite large near the discontinuities of the solution and lead to instability. To resolve this issue, Zhao et al. [31,32] adopted the idea of limiters for the discontinuous Galerkin (DG) method [4] to first modify the first order moments near the discontinuities of the solution, then, the same polynomials to approximate the numerical fluxes of the original PDE and the equations satisfied by the first order moments were used. It was found that the approach with modifications for the first order moments had better performance to eliminate the nonlinear oscillations than the other HWENO schemes. A more robust HWENO scheme was obtained in [31,32]. Motivated by this approach, we apply modifications of the derivatives of the solution by Hermite interpolations here in the finite difference HWENO scheme.

The algorithm of the proposed modified HWENO scheme in this paper has the following two major steps. At first, we modify the derivatives of the solution by the HWENO method based on its Hermite interpolation. Then the same stencils and polynomials are used to reconstruct the numerical fluxes of the original PDE and the equations satisfied by the derivatives. For the systems of hyperbolic conservation laws, all HWENO reconstructions are performed on local characteristic directions to avoid spurious oscillations as that in the classical fifth order finite difference WENO scheme [11]. Comparing with the original finite difference HWENO scheme [15], we do not need to use positivity-preserving flux limiter methodology, and the new method allows for larger CFL numbers. The effect of using modifications of the derivatives of the solution to eliminate the non-physical oscillations near the discontinuities will be shown in Example 3.7 of Sect. 3. Higher order numerical accuracy than the original finite difference HWENO scheme is achieved for two-dimensional problems in the case of using the same stencil and information for approximations. In addition, we also make the comparison of the proposed modified fifth order finite difference HWENO method with the classical fifth order finite difference WENO method [11], and it is found that the modified HWENO scheme has less numerical errors and higher resolution under the same conditions. It is noticed that the modified HWENO scheme needs a little more computational cost than that of WENO schemes for the same meshes, but it is much more compact as only immediate neighbor information is used in the reconstructions. In summary, the proposed modified finite difference HWENO scheme preserves the compactness and high resolution of the original finite difference HWENO scheme [15], while it is much more robust and has higher order numerical accuracy in solving two-dimensional problems as that shown in the numerical experiments.

The organization of the paper is as the following. In Sect. 2, we present the detailed construction of the modified finite difference HWENO scheme in one-dimensional and two-dimensional cases, respectively. In Sect. 3, numerical tests for problems with both smooth and non-smooth solutions are performed to illustrate the numerical accuracy, high resolution and robustness of the proposed scheme. Concluding remarks are given in Sect. 4.

2 A Modified Fifth Order Finite Difference HWENO Scheme

In this section, we design a modified HWENO scheme in the finite difference framework for hyperbolic conservation laws. The scheme has the fifth order accuracy for both one-dimensional and two-dimensional problems, while the original finite difference HWENO

scheme [15] only has fourth order accuracy for the two-dimensional problems, using the same stencil in the spatial discretization.

2.1 One-Dimensional Case

We first consider one-dimensional scalar hyperbolic conservation laws

$$\begin{cases} u_t + f(u)_x = 0, \\ u(x, 0) = u_0(x). \end{cases} \tag{2.1}$$

In the finite difference framework, the spatial domain is partitioned by uniform grid points $\{x_i\}$, and x_i is the center of the cell I_i . The boundary of I_i is $x_{i+1/2} = x_i + \Delta x/2$, where Δx is the grid size $x_{i+1} - x_i$. In order to design a Hermite WENO scheme, we take partial derivative w.r.t the variable x on both sides of the governing equation (2.1) and denote the partial derivative of $u(x, t)$ w.r.t x by a new function $v(x, t)$. Then, we obtain the following equations

$$\begin{cases} u_t + f(u)_x = 0, & u(x, 0) = u_0(x), \\ v_t + h(u, v)_x = 0, & v(x, 0) = v_0(x), \end{cases} \tag{2.2}$$

where $h(u, v) = f(u)_x = f'(u)u_x = f'(u)v$, and $v(x, 0) = u_x(x, 0)$. As that in [15,16] by Liu and Qiu, the semi-discrete finite difference scheme of (2.2) is

$$\begin{cases} \frac{du_i(t)}{dt} = -\frac{1}{\Delta x} (\hat{f}_{i+1/2} - \hat{f}_{i-1/2}), \\ \frac{dv_i(t)}{dt} = -\frac{1}{\Delta x} (\hat{h}_{i+1/2} - \hat{h}_{i-1/2}). \end{cases} \tag{2.3}$$

Here, $\hat{f}_{i+1/2}$ and $\hat{h}_{i+1/2}$ are the numerical fluxes which are the fifth order approximation of $\Phi_{i+1/2} = \Phi(x_{i+1/2})$ and $\Psi_{i+1/2} = \Psi(x_{i+1/2})$, respectively, where $\Phi(x)$ and $\Psi(x)$ are defined implicitly as that in [11,15,16]:

$$f(u(x)) = \frac{1}{\Delta x} \int_{x-\Delta x/2}^{x+\Delta x/2} \Phi(x)dx, \quad h(u(x), v(x)) = \frac{1}{\Delta x} \int_{x-\Delta x/2}^{x+\Delta x/2} \Psi(x)dx.$$

For the stability of the finite difference HWENO scheme, we split the fluxes $f(u)$ and $h(u, v)$ into two parts: $f(u) = f^+(u) + f^-(u)$ and $h(u, v) = h^+(u, v) + h^-(u, v)$, where $\frac{df^+(u)}{du} \geq 0$, $\frac{\partial h^+(u,v)}{\partial v} \geq 0$ and $\frac{df^-(u)}{du} \leq 0$, $\frac{\partial h^-(u,v)}{\partial v} \leq 0$, respectively. Here, the global Lax-Friedrichs flux splitting method is applied as

$$f^\pm(u) = \frac{1}{2}(f(u) \pm \alpha u) \quad \text{and} \quad h^\pm(u, v) = \frac{1}{2}(h(u, v) \pm \alpha v),$$

where α is defined as $\max_u |f'(u)|$. The numerical fluxes $\hat{f}_{i+1/2}^\pm$ and $\hat{h}_{i+1/2}^\pm$ are associated with the fluxes $f^\pm(u)$ and $h^\pm(u, v)$, respectively, where $\hat{f}_{i+1/2}^\pm = \hat{f}_{i+1/2}^+ + \hat{f}_{i+1/2}^-$ and $\hat{h}_{i+1/2}^\pm = \hat{h}_{i+1/2}^+ + \hat{h}_{i+1/2}^-$.

Next, we describe the detailed reconstruction procedure for the numerical fluxes $\hat{f}_{i+1/2}^\pm$ and $\hat{h}_{i+1/2}^\pm$. Again, unlike the origin finite difference HWENO scheme [15], we first modify the derivative of the solution by the HWENO method, based on its Hermite interpolation. The reconstruction procedure is consisted of the following two steps.

Step 1. Modify the derivative of the solution.

Since the solution for hyperbolic conservation laws often contains discontinuities and the derivative of the solution is quite large near discontinuities, we need to control its derivative

value. This idea comes from Zhao et al. [31,32], in which the first order moment of the solution is modified in advance near the discontinuities. Although a modification for the derivative of the solution adds extra computational costs to the algorithm, we reduce the computational costs in the original HWENO scheme by using the same polynomials to reconstruct $\hat{f}_{i+1/2}^{\pm}$ and $\hat{h}_{i+1/2}^{\pm}$ in the following Step 2. Furthermore, a larger CFL number such as 0.6 can be used in the new method, while the original finite difference HWENO scheme [15] needs to use a much smaller CFL number such as 0.2 for the stability of the method. This modification step is important in order to eliminate the non-physical spurious oscillations as that shown in our numerical experiments. Then there is no need to add the positivity-preserving flux limiter [9] as that in the original finite difference HWENO scheme [15].

Give three small stencils $S_1 = \{x_{i-1}, x_i\}$, $S_2 = \{x_{i-1}, x_i, x_{i+1}\}$, $S_3 = \{x_i, x_{i+1}\}$, and a big stencil $S_0 = \{S_1, S_2, S_3\} = S_2$, then, we first construct three quadratic polynomials $p_1(x)$, $p_2(x)$, $p_3(x)$ on S_1, S_2, S_3 by Hermite interpolation, respectively. They satisfy the following conditions

$$\begin{aligned} p_1(x_{i+l}) &= u_{i+l}, \quad l = -1, 0, & p_1'(x_{i-1}) &= v_{i-1}, \\ p_2(x_{i+l}) &= u_{i+l}, \quad l = -1, 0, 1, \\ p_3(x_{i+l}) &= u_{i+l}, \quad l = 0, 1, & p_3'(x_{i+1}) &= v_{i+1}. \end{aligned}$$

Also a quartic polynomial $p_0(x)$ is constructed on S_0 by Hermite interpolation, which satisfies

$$p_0(x_{i+l}) = u_{i+l}, \quad l = -1, 0, 1, \quad p_0'(x_{i+l}) = v_{i+l}, \quad l = -1, 1.$$

Then, their derivative values at x_i are evaluated and we have

$$\begin{aligned} p_1'(x_i) &= -v_{i-1} + \frac{2(u_i - u_{i-1})}{\Delta x}, \\ p_2'(x_i) &= \frac{u_{i+1} - u_{i-1}}{2\Delta x}, \\ p_3'(x_i) &= -v_{i+1} + \frac{2(u_{i+1} - u_i)}{\Delta x}, \\ p_0'(x_i) &= -\frac{v_{i-1} + v_{i+1}}{4} + \frac{3(u_{i+1} - u_{i-1})}{4\Delta x}. \end{aligned}$$

The linear weights $\gamma_1 = \frac{1}{4}$, $\gamma_2 = \frac{1}{2}$ and $\gamma_3 = \frac{1}{4}$ are obtained by requiring that

$$p_0'(x_i) = \sum_{n=1}^3 \gamma_n p_n'(x_i).$$

Next, we compute the smoothness indicators β_n to measure how smooth the functions $p_n(x)$ are in the target cell I_i , using the same definition as in [11,22],

$$\beta_n = \sum_{\alpha=1}^r \int_{I_i} \Delta x^{2\alpha-1} \left(\frac{d^\alpha p_n(x)}{dx^\alpha} \right)^2 dx, \quad n = 1, 2, 3. \tag{2.4}$$

Here $r = 2$ is the degree of the polynomials $p_n(x)$. The explicit formulas are

$$\begin{cases} \beta_1 = (2u_i - 2u_{i-1} - v_{i-1}\Delta x)^2 + \frac{13}{3}(u_i - u_{i-1} - v_{i-1}\Delta x)^2, \\ \beta_2 = \frac{1}{4}(u_{i+1} - u_{i-1})^2 + \frac{13}{12}(u_{i-1} - 2u_i + u_{i+1})^2, \\ \beta_3 = (2u_{i+1} - 2u_i - v_{i+1}\Delta x)^2 + \frac{13}{3}(u_{i+1} - u_i - v_{i+1}\Delta x)^2. \end{cases}$$

Now, the nonlinear weights are obtained as

$$\omega_n = \frac{\bar{\omega}_n}{\sum_{l=1}^3 \bar{\omega}_l}, \text{ with } \bar{\omega}_n = \frac{\gamma_n}{(\beta_n + \varepsilon)^2}, \quad n = 1, 2, 3,$$

where ε is set as 10^{-6} to avoid the denominator being zero. At last, the derivative value v_i is modified by

$$v_i^{new} = \sum_{n=1}^3 \omega_n p'_n(x_i).$$

v_i^{new} is the modified value of v at the point x_i .

Step 2. Reconstruct the numerical fluxes $\hat{f}_{i+1/2}^\pm$ and $\hat{h}_{i+1/2}^\pm$.

For simplicity, we only give the detailed reconstruction procedures for $\hat{f}_{i+1/2}^+$ and $\hat{h}_{i+1/2}^+$, while the formulas for the negative part of numerical fluxes $\hat{f}_{i+1/2}^-$ and $\hat{h}_{i+1/2}^-$ are mirror symmetric with respect to $x_{i+1/2}$ of that for $\hat{f}_{i+1/2}^+$ and $\hat{h}_{i+1/2}^+$, respectively. Again, we would like to emphasize that the modified HWENO scheme uses the same stencils and polynomials to reconstruct $\hat{f}_{i+1/2}^+$ and $\hat{h}_{i+1/2}^+$, and it is different from the original finite difference HWENO scheme [15].

We use the same stencils S_1, S_2, S_3 and S_0 given in Step 1 to reconstruct three cubic polynomials $p_1(x), p_2(x), p_3(x)$ on S_1, S_2, S_3 and a quintic polynomial $p_0(x)$ on S_0 , respectively, which satisfy

$$\begin{aligned} \frac{1}{\Delta x} \int_{I_{i+l}} p_1(x) dx &= f^+(u_{i+l}), \quad l = -1, 0, & \frac{1}{\Delta x} \int_{I_{i-1}} p'_1(x) dx &= h^+(u_{i-1}, v_{i-1}), \\ \frac{1}{\Delta x} \int_{I_i} p'_1(x) dx &= h^+(u_i, v_i^{new}), \\ \frac{1}{\Delta x} \int_{I_{i+l}} p_2(x) dx &= f^+(u_{i+l}), \quad l = -1, 0, 1, & \frac{1}{\Delta x} \int_{I_i} p'_2(x) dx &= h^+(u_i, v_i^{new}), \\ \frac{1}{\Delta x} \int_{I_{i+l}} p_3(x) dx &= f^+(u_{i+l}), \quad l = 0, 1, & \frac{1}{\Delta x} \int_{I_{i+1}} p'_3(x) dx &= h^+(u_{i+1}, v_{i+1}), \\ \frac{1}{\Delta x} \int_{I_i} p'_3(x) dx &= h^+(u_i, v_i^{new}), \end{aligned} \tag{2.5}$$

and

$$\begin{aligned} \frac{1}{\Delta x} \int_{I_{i+l}} p_0(x) dx &= f^+(u_{i+l}), \quad l = -1, 0, 1, & \frac{1}{\Delta x} \int_{I_{i\pm 1}} p'_0(x) dx &= h^+(u_{i\pm 1}, v_{i\pm 1}), \\ \frac{1}{\Delta x} \int_{I_i} p'_0(x) dx &= h^+(u_i, v_i^{new}), \end{aligned} \tag{2.6}$$

and in the next procedures, $f^+(u_{i+l})$ and $h^+(u_{i\pm 1}, v_{i\pm 1})$ would be simplified as f_{i+l}^+ and $h_{i\pm 1}^+$, respectively, and $h^+(u_i, v_i^{new})$ is also simplified as h_i^+ .

Remark 1 The reconstruction of the numerical flux $\hat{f}_{i+1/2}^+$ uses the numerical values $\{u_{i-1}, u_i, u_{i+1}\}$ and their derivatives $\{v_{i-1}, v_i^{new}, v_{i+1}\}$, shown in (2.5) and (2.6). Here v_i^{new} represents the modified value of v at the point x_i , while $v_{i\pm 1}$ are still the original derivatives at the points $x_{i\pm 1}$. Hence, the reconstruction of $\hat{f}_{i+1/2}^+$ only uses the numerical values and their derivatives at $\{x_{i-1}, x_i, x_{i+1}\}$, which preserves the nice property of compactness of the HWENO schemes.

Note that the reconstructions for $\hat{f}_{i+1/2}^+$ and $\hat{h}_{i+1/2}^+$ use the same smoothness indicators, then, we first compute the smoothness indicators β_n , which measure how smooth the functions $p_n(x)$ are on the cell I_i , by using the formula of the smoothness indicators (2.4). The explicit expressions are

$$\left\{ \begin{aligned} \beta_1 &= (h_i^+ \Delta x)^2 + \frac{13}{3} [3(f_{i-1}^+ - f_i^+) + (h_{i-1}^+ + 2h_i^+) \Delta x]^2 \\ &\quad + \frac{781}{20} [2(f_{i-1}^+ - f_i^+) + (h_{i-1}^+ + h_i^+) \Delta x]^2, \\ \beta_2 &= (h_i^+ \Delta x)^2 + \frac{13}{3} (f_{i-1}^+ - 2f_i^+ + f_{i+1}^+)^2 \\ &\quad + \frac{781}{80} (f_{i-1}^+ - f_{i+1}^+ + 2h_i^+ \Delta x)^2, \\ \beta_3 &= (h_i^+ \Delta x)^2 + \frac{13}{3} [3(f_i^+ - f_{i+1}^+) + (2h_i^+ + h_{i+1}^+) \Delta x]^2 \\ &\quad + \frac{781}{20} [2(f_i^+ - f_{i+1}^+) + (h_i^+ + h_{i+1}^+) \Delta x]^2. \end{aligned} \right. \tag{2.7}$$

Step 2.1. Reconstruct the numerical flux $\hat{f}_{i+1/2}^+$.

Using (2.5) and (2.6), we compute the reconstructions of $\hat{f}_{i+1/2}^+$ by evaluating the values of these polynomials at the point $x_{i+1/2}$. Their explicit expressions are

$$\begin{aligned} p_1(x_{i+1/2}) &= \frac{1}{2} f_{i-1}^+ + \frac{1}{2} f_i^+ + \frac{1}{6} h_{i-1}^+ \Delta x + \frac{5}{6} h_i^+ \Delta x, \\ p_2(x_{i+1/2}) &= \frac{1}{12} f_{i-1}^+ + \frac{5}{6} f_i^+ + \frac{1}{12} f_{i+1}^+ + \frac{1}{2} h_i^+ \Delta x, \\ p_3(x_{i+1/2}) &= \frac{1}{2} f_i^+ + \frac{1}{2} f_{i+1}^+ + \frac{1}{6} h_i^+ \Delta x - \frac{1}{6} h_{i+1}^+ \Delta x, \\ p_0(x_{i+1/2}) &= \frac{11}{60} f_{i-1}^+ + \frac{19}{30} f_i^+ + \frac{11}{60} f_{i+1}^+ + \frac{1}{20} h_{i-1}^+ \Delta x + \frac{1}{2} h_i^+ \Delta x - \frac{1}{20} h_{i+1}^+ \Delta x. \end{aligned}$$

Then we find the linear weights γ_1, γ_2 and γ_3 by requiring that

$$p_0(x_{i+1/2}) = \sum_{n=1}^3 \gamma_n p_n(x_{i+1/2}),$$

which gives that $\gamma_1 = \frac{3}{10}, \gamma_2 = \frac{2}{5}$ and $\gamma_3 = \frac{3}{10}$. With the smoothness indicators $\{\beta_n\}_{n=1}^3$ computed in (2.7), the nonlinear weights are formulated as

$$\omega_n = \frac{\bar{\omega}_n}{\sum_{l=1}^3 \bar{\omega}_l}, \text{ with } \bar{\omega}_n = \frac{\gamma_n}{(\beta_n + \varepsilon)^2}, \quad n = 1, 2, 3,$$

where ε is a small positive number taken as 10^{-6} . The final reconstruction of $\hat{f}_{i+1/2}^+$ is given by

$$\hat{f}_{i+1/2}^+ = \sum_{n=1}^3 \omega_n p_n(x_{i+1/2}).$$

Step 2.2. Reconstruct the numerical flux $\hat{h}_{i+1/2}^+$.

Similarly, we first compute the derivative values of these polynomials at the point $x_{i+1/2}$ to have

$$\begin{aligned} p'_1(x_{i+1/2}) &= \frac{4f_{i-1}^+ - 4f_i^+}{\Delta x} + \frac{3}{2} h_{i-1}^+ + \frac{7}{2} h_i^+, \\ p'_2(x_{i+1/2}) &= \frac{f_{i-1}^+ - 4f_i^+ + 3f_{i+1}^+}{4\Delta x} + \frac{1}{2} h_i^+, \end{aligned}$$

$$\begin{aligned}
 p'_3(x_{i+1/2}) &= \frac{2f_{i+1}^+ - 2f_i^+}{\Delta x} - \frac{1}{2}h_i^+ - \frac{1}{2}h_{i+1}^+, \\
 p'_0(x_{i+1/2}) &= \frac{f_{i-1}^+ - 8f_i^+ + 7f_{i+1}^+}{4\Delta x} + \frac{1}{12}h_{i-1}^+ - \frac{1}{6}h_i^+ - \frac{5}{12}h_{i+1}^+.
 \end{aligned}$$

The linear weights γ_1, γ_2 and γ_3 are determined by requiring

$$p'_0(x_{i+1/2}) = \sum_{n=1}^3 \gamma_n p'_n(x_{i+1/2}),$$

which gives that $\gamma_1 = \frac{1}{18}, \gamma_2 = \frac{1}{9}$ and $\gamma_3 = \frac{5}{6}$. With the smoothness indicators $\{\beta_n\}_{n=1}^3$ calculated in (2.7), the nonlinear weights are formulated as

$$\omega_n = \frac{\bar{\omega}_n}{\sum_{l=1}^3 \bar{\omega}_l}, \text{ with } \bar{\omega}_n = \frac{\gamma_n}{(\beta_n + \varepsilon)^2}, \quad n = 1, 2, 3,$$

where ε is still taken as 10^{-6} . Finally, the reconstructed value of $\hat{h}_{i+1/2}^+$ is given by

$$\hat{h}_{i+1/2}^+ = \sum_{n=1}^3 \omega_n p'_n(x_{i+1/2}).$$

After the spatial discretization, the semi-discrete scheme (2.3) is solved by the third order TVD Runge-Kutta method [23] in time as the following

$$\begin{cases}
 U^{(1)} = U^n + \Delta t L(U^n), \\
 U^{(2)} = \frac{3}{4}U^n + \frac{1}{4}U^{(1)} + \frac{1}{4}\Delta t L(U^{(1)}), \\
 U^{(n+1)} = \frac{1}{3}U^n + \frac{2}{3}U^{(2)} + \frac{2}{3}\Delta t L(U^{(2)}),
 \end{cases} \tag{2.8}$$

where $U = (u, v^{new})^T$ for the one-dimensional case.

2.2 Two-Dimensional Case

In this section we consider the two-dimensional hyperbolic conservation laws

$$\begin{cases}
 u_t + f(u)_x + g(u)_y = 0, \\
 u(x, y, 0) = u_0(x, y).
 \end{cases} \tag{2.9}$$

For the simplicity of algorithm description, we focus on the scalar equation. The extension to a system of equations is straightforward. The computation domain is partitioned by a uniform mesh with grid points $\{(x_i, y_j)\}$, and grid sizes $\Delta x = x_{i+1} - x_i$ and $\Delta y = y_{j+1} - y_j$. The half grid points $x_{i+1/2} = x_i + \Delta x/2$ and $y_{j+1/2} = y_j + \Delta y/2$. The computation cell $I_{i,j}$ is defined by $[x_{i-1/2}, x_{i+1/2}] \times [y_{j-1/2}, y_{j+1/2}]$, and (x_i, y_j) is the center of the cell $I_{i,j}$. To design a Hermite WENO scheme, we take the partial derivatives of the governing equation (2.9) with respect to the x and y variables, respectively, and introduce new variables $v = u_x$ and $w = u_y$, then obtain the following equations

$$\begin{cases}
 u_t + f(u)_x + g(u)_y = 0, & u(x, y, 0) = u_0(x, y), \\
 v_t + h(u, v)_x + r(u, v)_y = 0, & v(x, y, 0) = v_0(x, y), \\
 w_t + q(u, w)_x + s(u, w)_y = 0, & w(x, y, 0) = w_0(x, y),
 \end{cases} \tag{2.10}$$

where

$$\begin{aligned}
 h(u, v) &= f'(u)v, \quad r(u, v) = g'(u)v, \quad v(x, y, 0) = u_x(x, y, 0); \\
 q(u, w) &= f'(u)w, \quad s(u, w) = g'(u)w, \quad w(x, y, 0) = u_y(x, y, 0).
 \end{aligned}$$

We can notice that the Eqs. (2.2) and (2.10) have the similar form, such as $f(u)_x$ and $g(u)_y$ are related to $h(u, v)_x$ and $s(u, w)_y$, respectively. Therefore, we can extend the methodology from one-dimensional case to approximate these four terms, but the mixed derivative terms $q(u, w)_x$ and $r(u, v)_y$ are hard to approximate like one-dimensional case. Hence, we would only introduce how to approximate the mixed derivative terms here. Just like one-dimensional case, we first give the semi-discrete finite difference scheme of (2.10) following as

$$\begin{cases} \frac{du_{i,j}(t)}{dt} = -\frac{1}{\Delta x} \left(\hat{f}_{i+1/2,j} - \hat{f}_{i-1/2,j} \right) - \frac{1}{\Delta y} \left(\hat{g}_{i,j+1/2} - \hat{g}_{i,j-1/2} \right), \\ \frac{dv_{i,j}(t)}{dt} = -\frac{1}{\Delta x} \left(\hat{h}_{i+1/2,j} - \hat{h}_{i-1/2,j} \right) - \frac{1}{\Delta y} \left(\hat{r}_{i,j+1/2} - \hat{r}_{i,j-1/2} \right), \\ \frac{dw_{i,j}(t)}{dt} = -\frac{1}{\Delta x} \left(\hat{q}_{i+1/2,j} - \hat{q}_{i-1/2,j} \right) - \frac{1}{\Delta y} \left(\hat{s}_{i,j+1/2} - \hat{s}_{i,j-1/2} \right). \end{cases} \tag{2.11}$$

Here, the numerical fluxes $\hat{f}_{i\pm 1/2,j}$, $\hat{h}_{i\pm 1/2,j}$, $\hat{g}_{i,j\pm 1/2}$ and $\hat{s}_{i,j\pm 1/2}$ are reconstructed in a dimension-by-dimensional manner by adding a modification methodology for the partial derivatives in the x and y directions in advance. The mixed derivative terms $\hat{q}_{i\pm 1/2,j}$ and $\hat{r}_{i,j\pm 1/2}$ would be reconstructed by linear approximation for we have modified the partial derivatives $v_{i,j}$ and $w_{i,j}$ for all points.

The general frameworks for the spatial discretization are: in Step 3, we modify the partial derivative values in the x and y directions, respectively; then, in Step 4, we introduce the main procedures to reconstruct the numerical fluxes.

Step 3. Modify the partial derivative of the solution.

We would modify the partial derivative values in the x and y directions denoted by dimension by dimension, respectively, and the explicit procedures have been introduced in Step 1 for one-dimensional problems. Also, the modified values of v and w at the point (x_i, y_j) are represented as $v_{i,j}^{new}$ and $w_{i,j}^{new}$ in the next procedures, respectively.

Step 4. Reconstruct the numerical fluxes $\hat{f}_{i\pm 1/2,j}$, $\hat{h}_{i\pm 1/2,j}$, $\hat{g}_{i,j\pm 1/2}$, $\hat{s}_{i,j\pm 1/2}$, $\hat{q}_{i\pm 1/2,j}$ and $\hat{r}_{i,j\pm 1/2}$.

The numerical fluxes $\hat{f}_{i\pm 1/2,j}$, $\hat{h}_{i\pm 1/2,j}$, $\hat{g}_{i,j\pm 1/2}$ and $\hat{s}_{i,j\pm 1/2}$ are reconstructed in a dimension-by-dimensional manner, and the procedures are similar to one-dimensional case introduced in Step 2. For the mixed derivative terms $\hat{q}_{i\pm 1/2,j}$ and $\hat{r}_{i,j\pm 1/2}$, there's no need to split the fluxes $q(u, w)$ and $r(u, v)$, and they would be reconstructed by the linear approximation straightforwardly, as we have modified the partial derivatives of the solution in Step 3, while the original finite difference HWENO scheme [15] needed to split the fluxes $q(u, w)$ and $r(u, v)$ and used the third order WENO method to overcome the non-physical oscillations, which leads to the HWENO scheme [15] only has fourth order accuracy in the two-dimensional case.

In the next procedures, we only introduce the reconstruction for $\hat{q}_{i+1/2,j}$ in detail, and $q(u_{i,j}, w_{i,j}^{new})$ is simplified as $q_{i,j}$. The reconstruction for $\hat{r}_{i,j+1/2}$ is similar, which would not be presented repeatedly.

We first give the stencil $S_0 = \{x_{i-1}, x_i, x_{i+1}, x_{i+2}\}$, then we get a cubic polynomial $p_0(x)$ on S_0 , satisfying

$$\frac{1}{\Delta x} \int_{x_{i+k-1/2}}^{x_{i+k+1/2}} p_0(x)dx = q_{i+k,j}, \quad k = -1, 0, 1, 2,$$

then, we can easily obtain the linear approximation for $\hat{q}_{i+1/2,j}$ as

$$\hat{q}_{i+1/2,j} = p_0(x_{i+1/2}) = \frac{1}{12} (-q_{i-1,j} + 7q_{i,j} + 7q_{i+1,j} - q_{i+2,j}). \quad (2.12)$$

After we finish the spatial discretization, the semi-discrete scheme (2.11) is discretized in time by the third order TVD Runge-Kutta method, and the explicit expression is presented in (2.8) with $U = (u, v^{new}, w^{new})^T$ for two-dimensional case.

Remark 2 For the two-dimensional cases, the mixed derivative $\hat{q}_{i+1/2,j}$ is reconstructed directly by the linear scheme (2.12). The partial derivatives of the solution have been modified by HWENO methodology at all points in Step 3, and it is interesting to observe that the linear reconstruction for the mixed derivative does not lead to any spurious oscillations in the numerical experiments as shown in the next section.

Remark 3 For the system case, such as the one-dimensional and two-dimensional compressible Euler equations, all HWENO procedures are implemented with a local characteristic field decomposition as in [11], while the linear approximation is performed using the component by component approach.

3 Numerical Experiments

In this section, we perform the numerical experiments to test the modified finite difference HWENO scheme by solving various one-dimensional and two-dimensional problems. The numerical results of the proposed fifth order finite difference HWENO scheme are compared to that by the classical fifth order finite difference WENO scheme of Jiang and Shu [11] and the original finite difference HWENO scheme of Liu and Qiu [15] without the positivity-preserving flux limiter [9], to highlight the new properties of the new scheme. The CFL number for the new modified HWENO scheme and the classical WENO scheme [11] in the numerical experiments is set as 0.6, while for the original finite difference HWENO scheme [15], a smaller CFL number such as 0.2 has to be used. Also the original finite difference HWENO scheme [15] can only achieve fourth order accuracy for two-dimensional problems while our new scheme enhances the accuracy order to the fifth order based on the same stencil of the scheme.

Here in this section, we use the modified HWENO scheme to denote the new modified finite difference HWENO scheme developed in this paper, and use the classical WENO scheme to represent the classical fifth order finite difference WENO scheme [11]. In addition, we use the original HWENO scheme to denote the original finite difference HWENO scheme [15] without the positivity-preserving flux limiter [9].

3.1 Smooth Problems

Example 3.1 We solve the one-dimensional Burgers' equation:

$$u_t + \left(\frac{u^2}{2} \right)_x = 0, \quad 0 < x < 2. \quad (3.1)$$

The initial condition is $u(x, 0) = 0.5 + \sin(\pi x)$ with periodic boundary condition. The final time is $T = 0.5/\pi$, when the solution is still smooth. We present the numerical errors and orders in Table 1 for the WENO and HWENO schemes. It is seen that the WENO

Table 1 1D-Burgers’ equation: initial data $u(x, 0) = 0.5 + \sin(\pi x)$. WENO and HWENO schemes. $T = 0.5/\pi$. L^1 and L^∞ errors and orders

Grid points	Classical WENO scheme				Original HWENO scheme			
	L^1 error	Order	L^∞ error	Order	L^1 error	Order	L^∞ error	Order
10	1.90E−02		7.46E−02		1.48E−02		6.58E−02	
20	2.06E−03	3.20	1.23E−02	2.60	1.19E−03	3.63	7.96E−03	3.05
40	1.22E−04	4.08	1.05E−03	3.55	5.10E−05	4.55	4.79E−04	4.05
80	4.36E−06	4.80	4.78E−05	4.46	1.66E−06	4.94	1.68E−05	4.84
160	1.64E−07	4.74	1.41E−06	5.09	6.07E−08	4.77	6.53E−07	4.69
320	4.78E−09	5.10	7.35E−08	4.26	1.74E−09	5.13	3.20E−08	4.35

Grid points	Modified HWENO scheme			
	L^1 error	Order	L^∞ error	Order
10	6.39E−03		3.00E−02	
20	5.67E−04	3.49	4.04E−03	2.90
40	3.18E−05	4.16	3.85E−04	3.39
80	1.35E−06	4.56	1.31E−05	4.88
160	5.32E−08	4.67	5.67E−07	4.53
320	1.55E−09	5.10	2.06E−08	4.78

and HWENO schemes all achieve designed fifth order accuracy, but the modified HWENO scheme has smaller L^1 and L^∞ errors than the classical WENO and the original HWENO schemes on the same mesh. In addition, the original HWENO and the modified HWENO schemes only need a compact three-point stencil while the classical WENO scheme needs a five-point stencil in the reconstructions.

Example 3.2 We consider the one-dimensional Euler system of equations:

$$\frac{\partial}{\partial t} \begin{pmatrix} \rho \\ \rho\mu \\ E \end{pmatrix} + \frac{\partial}{\partial x} \begin{pmatrix} \rho\mu \\ \rho\mu^2 + p \\ \mu(E + p) \end{pmatrix} = 0, \tag{3.2}$$

in which ρ is density, μ is velocity, E is total energy and p is pressure. The initial conditions are $\rho(x, 0) = 1 + 0.2 \sin(\pi x)$, $\mu(x, 0) = 1$, $p(x, 0) = 1$ and $\gamma = 1.4$. Periodic boundary conditions are applied here. The computational domain is $x \in [0, 2\pi]$, and the final time is $T = 2$. The exact solution is $\rho(x, T) = 1 + 0.2 \sin(\pi(x - T))$, $\mu(x, 0) = 1$, $p(x, 0) = 1$. We list the numerical errors and accuracy orders of the density for the WENO and HWENO schemes in Table 2. It shows that these schemes achieve designed fifth order accuracy. Again, the modified HWENO scheme has smaller numerical errors than the classical WENO and the original HWENO schemes on the same mesh, and the original HWENO and the modified HWENO schemes are more compact than the classical WENO scheme because two HWENO schemes only need three points while the classical WENO scheme needs five points in the spatial reconstructed stencil.

Table 2 1D-Euler equations: initial data $\rho(x, 0) = 1 + 0.2 \sin(\pi x)$, $\mu(x, 0) = 1$ and $p(x, 0) = 1$. WENO and HWENO schemes. $T = 2$. L^1 and L^∞ errors and orders

Grid points	Classical WENO scheme				Original HWENO scheme			
	L^1 error	Order	L^∞ error	Order	L^1 error	Order	L^∞ error	Order
10	1.13E-02		1.66E-02		5.50E-03		8.67E-03	
20	6.26E-04	4.17	9.94E-04	4.06	2.61E-04	4.40	4.39E-04	4.30
40	2.04E-05	4.94	3.72E-05	4.74	8.00E-06	5.03	1.55E-05	4.83
80	6.45E-07	4.98	1.21E-06	4.94	2.48E-07	5.01	4.81E-07	5.01
160	2.01E-08	5.01	3.67E-08	5.05	7.68E-09	5.01	1.43E-08	5.07
320	6.09E-10	5.04	1.01E-09	5.19	2.32E-10	5.05	3.85E-10	5.22

Grid points	Modified HWENO scheme			
	L^1 error	Order	L^∞ error	Order
10	5.64E-03		9.96E-03	
20	2.44E-04	4.53	4.43E-04	4.49
40	7.14E-06	5.09	1.40E-05	4.99
80	2.21E-07	5.01	4.37E-07	5.00
160	6.85E-09	5.01	1.25E-08	5.13
320	2.05E-10	5.06	3.53E-10	5.14

Example 3.3 We consider the two-dimensional Burgers' equation:

$$u_t + \left(\frac{u^2}{2}\right)_x + \left(\frac{u^2}{2}\right)_y = 0, \quad 0 < x < 4, \quad 0 < y < 4. \tag{3.3}$$

The initial condition is $u(x, y, 0) = 0.5 + \sin(\pi(x+y)/2)$ with periodic boundary conditions. The final time is $T = 0.5/\pi$, when the solution is still smooth. We show the numerical errors and accuracy orders in Table 3, which illustrates that the classical WENO and the modified HWENO schemes both have desired fifth order accuracy, while the original HWENO scheme only has fourth order accuracy. Similar to the previous examples, the modified HWENO scheme has better performance with smaller L^1 and L^∞ errors than the classical WENO and the original HWENO schemes on the same mesh, and the big stencil in the HWENO reconstruction only needs three points and is more compact than the classical WENO scheme.

Example 3.4 We solve the two-dimensional Euler system of equations:

$$\frac{\partial}{\partial t} \begin{pmatrix} \rho \\ \rho\mu \\ \rho\nu \\ E \end{pmatrix} + \frac{\partial}{\partial x} \begin{pmatrix} \rho\mu \\ \rho\mu^2 + p \\ \rho\mu\nu \\ \mu(E + p) \end{pmatrix} + \frac{\partial}{\partial y} \begin{pmatrix} \rho\nu \\ \rho\mu\nu \\ \rho\nu^2 + p \\ \nu(E + p) \end{pmatrix} = 0, \tag{3.4}$$

where ρ is the density, (μ, ν) is the velocity, E is the total energy and p is the pressure. The initial conditions are $\rho(x, y, 0) = 1 + 0.2 \sin(\pi(x+y))$, $\mu(x, y, 0) = 0.7$, $\nu(x, y, 0) = 0.3$, $p(x, y, 0) = 1$ and $\gamma = 1.4$. The computational domain is $(x, y) \in [0, 2] \times [0, 2]$. Periodic boundary conditions are applied in each direction. The final time is $T = 2$, and the exact solution of ρ is $\rho(x, y, T) = 1 + 0.2 \sin(\pi(x+y-T))$. The numerical errors and accuracy orders of the density for the WENO and HWENO schemes are presented in Table 4. Again

Table 3 2D-Burgers' equation: initial data $u(x, y, 0) = 0.5 + \sin(\pi(x+y)/2)$. WENO and HWENO schemes. $T = 0.5/\pi$. L^1 and L^∞ errors and orders

Grid points	Classical WENO scheme				Original HWENO scheme			
	L^1 error	Order	L^∞ error	Order	L^1 error	Order	L^∞ error	Order
10×10	2.07E-02		7.50E-02		6.41E-02		6.94E-02	
20×20	2.17E-03	3.25	1.21E-02	2.63	5.47E-03	3.55	6.74E-03	3.36
40×40	1.28E-04	4.09	1.04E-03	3.54	8.13E-04	2.75	9.19E-04	2.87
80×80	4.47E-06	4.83	4.73E-05	4.46	1.97E-04	2.05	6.23E-04	0.56
160×160	1.65E-07	4.76	1.39E-06	5.09	1.02E-05	4.27	5.37E-05	3.54
320×320	4.78E-09	5.11	7.28E-08	4.25	9.28E-08	6.77	4.08E-07	7.04
Grid points	Modified HWENO scheme							
	L^1 error	Order	L^∞ error	Order				
10×10	6.92E-03		3.01E-02					
20×20	5.91E-04	3.55	3.98E-03	2.92				
40×40	3.22E-05	4.20	3.82E-04	3.38				
80×80	1.35E-06	4.57	1.29E-05	4.89				
160×160	5.30E-08	4.67	5.65E-07	4.51				
320×320	1.54E-09	5.11	2.05E-08	4.78				

we see that the classical WENO and the modified HWENO schemes have designed fifth order accuracy, while the original HWENO scheme only has fourth order accuracy, and the modified HWENO scheme has smaller L^1 and L^∞ errors than the classical WENO and the original HWENO schemes on the same mesh. In addition, two HWENO schemes are much more compact as only immediate neighbor information is used in the reconstructions.

3.2 Non-smooth Problems

Example 3.5 We solve the one-dimensional Burgers' equation (3.1) given in Example 3.1 with the same initial and boundary conditions, but the final time is $T = 1.5/\pi$ when the solution is discontinuous. The numerical solution and the exact solution are plotted in Fig. 1. We see that both the classical WENO and the modified HWENO schemes obtain the results which are free of the non-physical oscillations, while the original HWENO scheme still has slight oscillations even using smaller CFL number as the derivative of the solution near by discontinuities is directly used for the scheme, which would be quite large, and the modified HWENO scheme can overcome oscillations well through HWENO reconstructing the derivatives. In addition, the modified HWENO scheme has better resolution than the classical WENO scheme with slightly less transition points across the discontinuities.

Example 3.6 We solve a one-dimensional nonlinear non-convex scalar Buckley-Leverett problem:

$$u_t + \left(\frac{4u^2}{4u^2 + (1-u)^2} \right)_x = 0, \quad -1 \leq x \leq 1.$$

Table 4 2D-Euler equations: initial data $\rho(x, y, 0) = 1 + 0.2 \sin(\pi(x+y))$, $\mu(x, y, 0) = 0.7$, $v(x, y, 0) = 0.3$ and $p(x, y, 0) = 1$. WENO and HWENO schemes. $T = 2$. L^1 and L^∞ errors and orders

Grid points	Classical WENO scheme				Original HWENO scheme			
	L^1 error	Order	L^∞ error	Order	L^1 error	Order	L^∞ error	Order
10×10	1.94E-02		2.80E-02		3.32E-02		6.75E-02	
20×20	1.07E-03	4.18	1.53E-03	4.19	5.70E-03	2.54	1.82E-02	1.89
40×40	3.57E-05	4.91	6.06E-05	4.66	2.43E-03	1.23	7.27E-03	1.33
80×80	1.11E-06	5.00	2.01E-06	4.92	8.47E-06	8.17	2.91E-05	7.97
160×160	3.45E-08	5.02	6.22E-08	5.01	1.32E-07	6.00	2.84E-07	6.68
320×320	1.03E-09	5.06	1.73E-09	5.17	7.30E-09	4.18	1.74E-08	4.03

Grid points	Modified HWENO scheme			
	L^1 error	order	L^∞ error	Order
10×10	8.78E-03		1.38E-02	
20×20	3.84E-04	4.52	6.21E-04	4.47
40×40	1.13E-05	5.08	2.11E-05	4.88
80×80	3.47E-07	5.03	6.50E-07	5.02
160×160	1.07E-08	5.02	1.94E-08	5.07
320×320	3.20E-10	5.06	5.49E-10	5.14

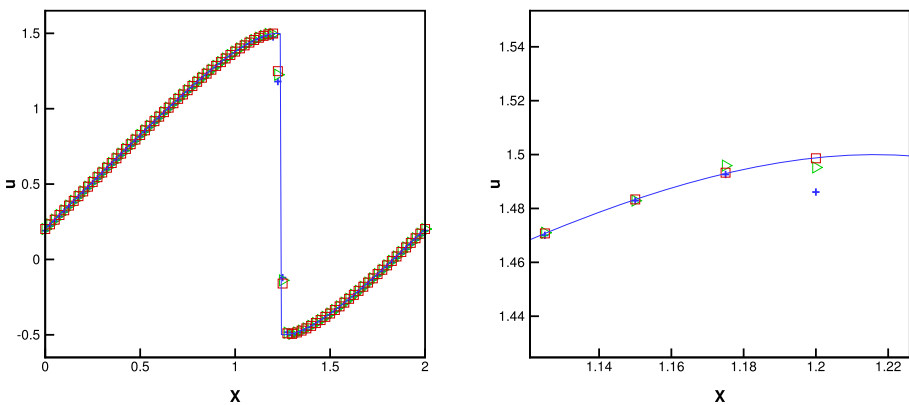


Fig. 1 1D-Burgers' equation: initial data $u(x, 0) = 0.5 + \sin(\pi x)$. $T = 1.5/\pi$. From left to right: the numerical results and its partial enlarged view. Black solid line: the exact solution; blue plus signs: the result of the classical WENO scheme; green triangles: the result of the original HWENO scheme; red squares: the result of the modified HWENO scheme. Grid points: 80

The initial condition is $u = 1$ for $-\frac{1}{2} \leq x \leq 0$ and $u = 0$ elsewhere with constant boundary conditions. The final time is $T = 0.4$. The exact solution of this problem contains both shock wave and rarefaction wave. It is a popular benchmark problem to test high-order numerical methods. If schemes are not carefully designed, they may converge to a non-physical solution which violates the entropy condition. The numerical results are presented in Fig. 2. We can see that the modified HWENO scheme performs well in capturing the correct entropy solution as the classical WENO scheme, and the modified HWENO scheme

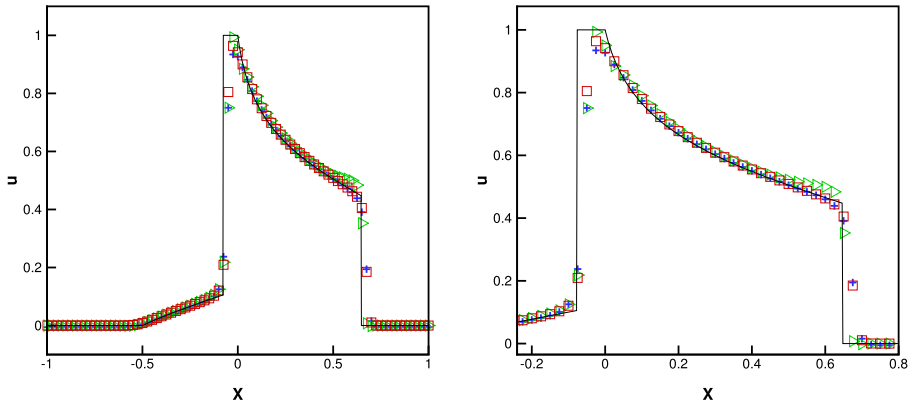


Fig. 2 1D Buckley-Leverett problem: initial data $u = 1$ for $-\frac{1}{2} \leq x \leq 0$ and $u = 0$ elsewhere. $T = 0.4$. From left to right: the numerical results and its partial enlarged view. Black solid line: the exact solution; blue plus signs: the result of the classical WENO scheme; green triangles: the result of the original HWENO scheme; red squares: the result of the modified HWENO scheme. Grid points: 80

shows slightly less dissipations and has better resolution than the classical WENO scheme. In addition, we can see the original HWENO scheme still has slight oscillations, while the modified HWENO scheme can control the non-physical oscillations well.

Example 3.7 We solve the one-dimensional Euler system of equations (3.2) with the following Riemann initial condition:

$$(\rho, \mu, p, \gamma)^T = \begin{cases} (0.445, 0.698, 3.528, 1.4)^T, & x \in [-0.5, 0), \\ (0.5, 0, 0.571, 1.4)^T, & x \in [0, 0.5]. \end{cases}$$

The final time is $T = 0.16$. The exact solution and the numerical results of density ρ using 200 grid points with a zoomed in picture are presented in Fig. 3. Both the classical WENO and the modified HWENO schemes generate a stable entropy solution. Again, due to the compactness of the HWENO scheme, the result computed by the modified HWENO scheme has better resolution than the classical WENO scheme. We also can see the result of the original HWENO scheme without the positivity-preserving flux limiter [9], shown by the green triangle symbols in Fig. 3. Obvious oscillations are observed and this can not be improved by using a smaller CFL number. The result shows that the positivity-preserving flux limiter is a key component to ensure the nonlinear stability of the original HWENO scheme. However the positivity-preserving flux limiter is not needed in the modified HWENO scheme of this paper, leading to a simpler and more robust scheme. In addition, to verify whether the modification for the derivative of the solution is necessary or not, we solve this problem by the method which does not modify the derivative of the solution in the modified HWENO scheme. The result is shown by the purple circle symbols in Fig. 3. Obvious non-physical oscillations are observed. This illustrates that the step of modification for the derivative of the numerical solution in the new HWENO scheme is significant and necessary to eliminate the non-physical oscillations and ensure the nonlinear stability of the scheme.

Example 3.8 We solve the following Shu-Osher problem, and the initial condition is

$$(\rho, \mu, p, \gamma)^T = \begin{cases} (3.857143, 2.629369, 10.333333, 1.4)^T, & x \in [-5, -4), \\ (1 + 0.2 \sin(5x), 0, 1, 1.4)^T, & x \in [-4, 5]. \end{cases}$$

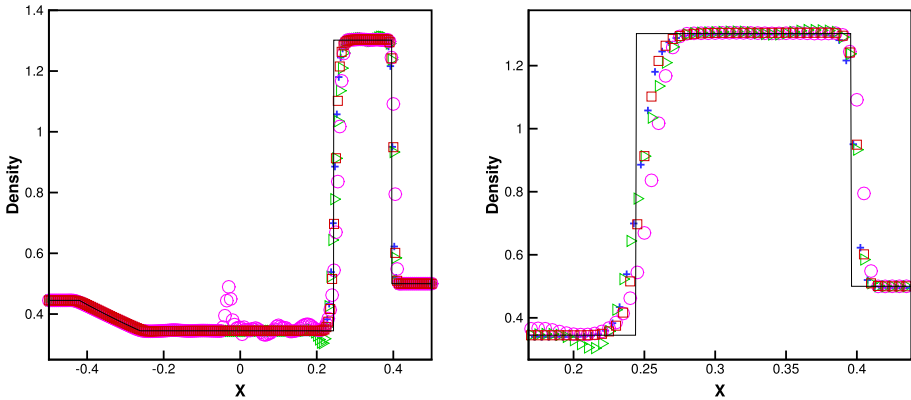


Fig. 3 The Lax problem. $T = 0.16$. From left to right: density; density zoomed in; Black solid line: the exact solution; blue plus signs: the result of the classical WENO scheme; green triangles: the result of the original HWENO scheme; red squares: the result of the modified HWENO scheme; purple circles: the result of the modified HWENO scheme with no modification procedure for the derivative of the solution. Grid points: 200

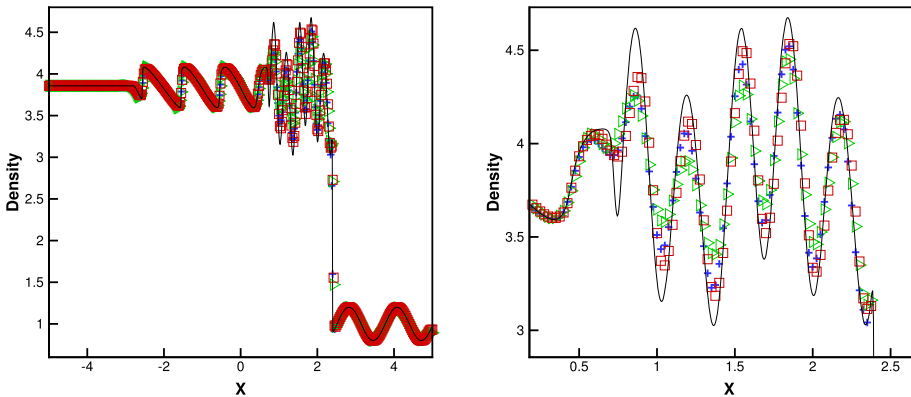


Fig. 4 The shock density wave interaction problem. $T = 1.8$. From left to right: density; density zoomed in. Black solid line: the exact solution; blue plus signs: the result of the classical WENO scheme; green triangles: the result of the original HWENO scheme; red squares: the result of the modified HWENO scheme. Grid points: 400

The final time is $T = 1.8$. The solution of this problem has a moving Mach 3 shock interacting with sine waves in density [22], and contains both shock waves and complex smooth region structures. We present the computed density ρ against the referenced “exact” solution and the zoomed in picture in Fig. 4. The referenced “exact” solution is computed by the fifth order finite difference WENO scheme [11] with 2000 grid points. It can be seen that the the modified HWENO scheme simulates this problem well, and it also has higher resolution than the classical WENO and the original HWENO schemes.

Example 3.9 We consider a problem of the interaction of two blast waves, and the initial condition is

$$(\rho, \mu, p, \gamma)^T = \begin{cases} (1, 0, 10^3, 1.4)^T, & 0 < x < 0.1, \\ (1, 0, 10^{-2}, 1.4)^T, & 0.1 < x < 0.9, \\ (1, 0, 10^2, 1.4)^T, & 0.9 < x < 1. \end{cases}$$

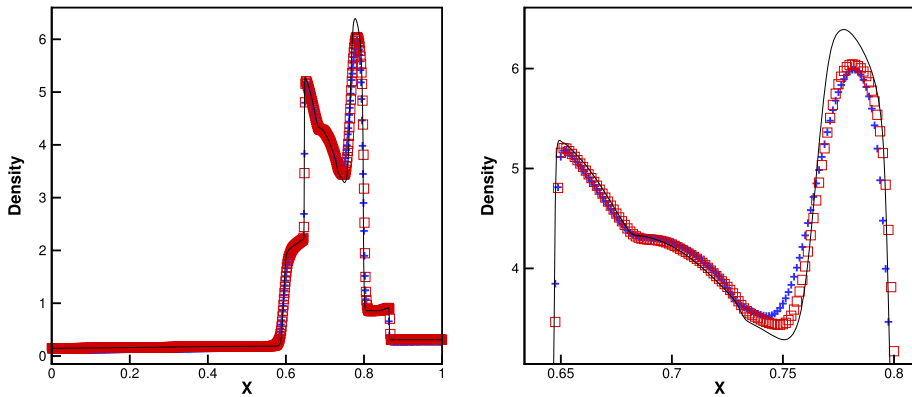


Fig. 5 The blast wave problem. $T = 0.038$. From left to right: density; density zoomed in. Black solid line: the exact solution; blue plus signs: the result of the classical WENO scheme; red squares: the result of the modified HWENO scheme. Grid points: 800

The final time T is 0.038 and the reflective condition is applied in two boundaries. The numerical results of the density by the WENO and HWENO schemes, the reference “exact” solution and the zoomed in picture are plotted in Fig. 5. The reference “exact” solution is obtained by a converged solution computed by the fifth order finite difference WENO scheme [11] with 2000 grid points. We see that the modified HWENO scheme generates a stable solution without non-physical oscillations. However, the original HWENO scheme fails to simulate this problem if the positivity-preserving flux limiter [9] is not used, even with a smaller CFL number. This shows that the modified HWENO scheme proposed in this paper is more robust than the original one [15]. Also, the new HWENO scheme has better resolution than the classical WENO scheme as shown in Fig. 5.

Example 3.10 We solve the two-dimensional Burgers’ equation (3.3) in Example 3.3 with the same initial and boundary conditions, and the final time is $T = 1.5/\pi$, when the solution is discontinuous. The numerical solutions computed by the WENO and HWENO schemes, along with the exact solution are presented in Fig. 6. Again, we see that the modified HWENO scheme has a slightly better resolution than the classical WENO and the original HWENO schemes.

Example 3.11 We solve the double Mach reflection problem from [27] modeled by the two-dimensional Euler system of equations (3.4). The computational domain is $([0, 4] \times [0, 1])$. $\gamma = 1.4$ and the final time is $T = 0.2$. This example has a reflection wall located at the bottom, starting from $x = \frac{1}{6}$, $y = 0$, making a 60° angle with the x -axis. At the bottom boundary, the exact post-shock condition is imposed from $x = 0$ to $x = \frac{1}{6}$ and the rest has the reflection boundary condition. At the top boundary, the exact motion of the Mach 10 shock is imposed. Inflow and outflow boundary conditions are applied for the left and right boundaries, respectively. In Fig. 7, we present the numerical results computed by the classical WENO and the modified HWENO schemes in the region $[0, 3] \times [0, 1]$ and the blow-up region around the double Mach stems. It is observed that the modified HWENO scheme generates a result with higher resolution than the classical WENO scheme, while the original HWENO scheme fails to simulate this problem if the positivity-preserving flux

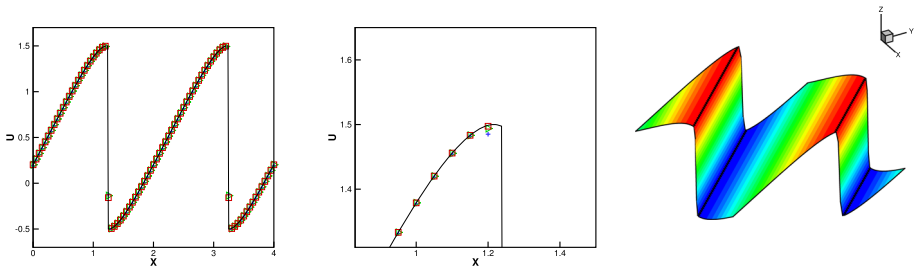


Fig. 6 2D-Burgers' equation: initial data $u(x, y, 0) = 0.5 + \sin(\pi(x + y)/2)$. $T = 1.5/\pi$. From left to right: the numerical solution at $x = y$, its partial enlarged view and the surface computed by the modified HWENO scheme. Black solid line: the exact solution; blue plus signs: the result of the classical WENO scheme; green triangles: the result of the original HWENO scheme; red squares: the result of the modified HWENO scheme. Grid points: 80×80

limiter [9] is not employed, even with a smaller CFL number, which illustrates that the modified HWENO scheme proposed in this paper is more robust than the original one [15].

Example 3.12 The problem is about a Mach 3 wind tunnel with a forward step [27] modeled by the two-dimensional Euler system of equations (3.4). In this problem, there is a wind tunnel with a initial right-going Mach 3 flow, and it has the width of 1 unit and the length of 3 units. The height of the step is 0.2 unit and it is located 0.6 length unit from the left-hand end of the tunnel. Reflective boundary conditions are applied along the wall of the tunnel. Inflow and outflow boundary conditions are applied at the entrance and the exit, respectively. The corner of the step is a singular point and we treat it as in [27]. We compute this problem till the time $T = 4$, and present the numerical results of the classical WENO and the modified HWENO schemes with 960×320 grid points in Fig. 8. It shows that the classical WENO and the modified HWENO schemes simulate this problem very well and they have comparable resolution for this problem. Again, the original HWENO scheme [15] fails to simulate this problem if the positivity-preserving flux limiter [9] is not applied, even with a smaller CFL number.

4 Concluding Remarks

In this paper, a modified fifth order finite difference Hermite weighted essentially non-oscillatory (HWENO) scheme is proposed for solving one-dimensional and two-dimensional hyperbolic conservation laws. Comparing with the original finite difference HWENO scheme [15], the modified HWENO scheme is simpler and more robust since we do not need to add a positivity-preserving flux limiter and use a smaller CFL number than the usual to ensure the stability of the scheme as in [15]. The new HWENO scheme has fifth order accuracy in solving both the one-dimensional and the two-dimensional problems, while based on the same reconstruction stencil the original finite difference HWENO scheme only has fourth order accuracy in solving the two-dimensional problems. Note that we develop an algorithm to modify the derivatives of the numerical solution in Step 1 and Step 3 of the scheme. This is a significant and necessary component in the scheme to eliminate the possible non-physical oscillations and ensure the nonlinear stability. Furthermore, we also make the comparison of the computational time for the WENO and HWENO schemes in the numerical tests, and it is found that the modified HWENO scheme uses less computational cost than the original one

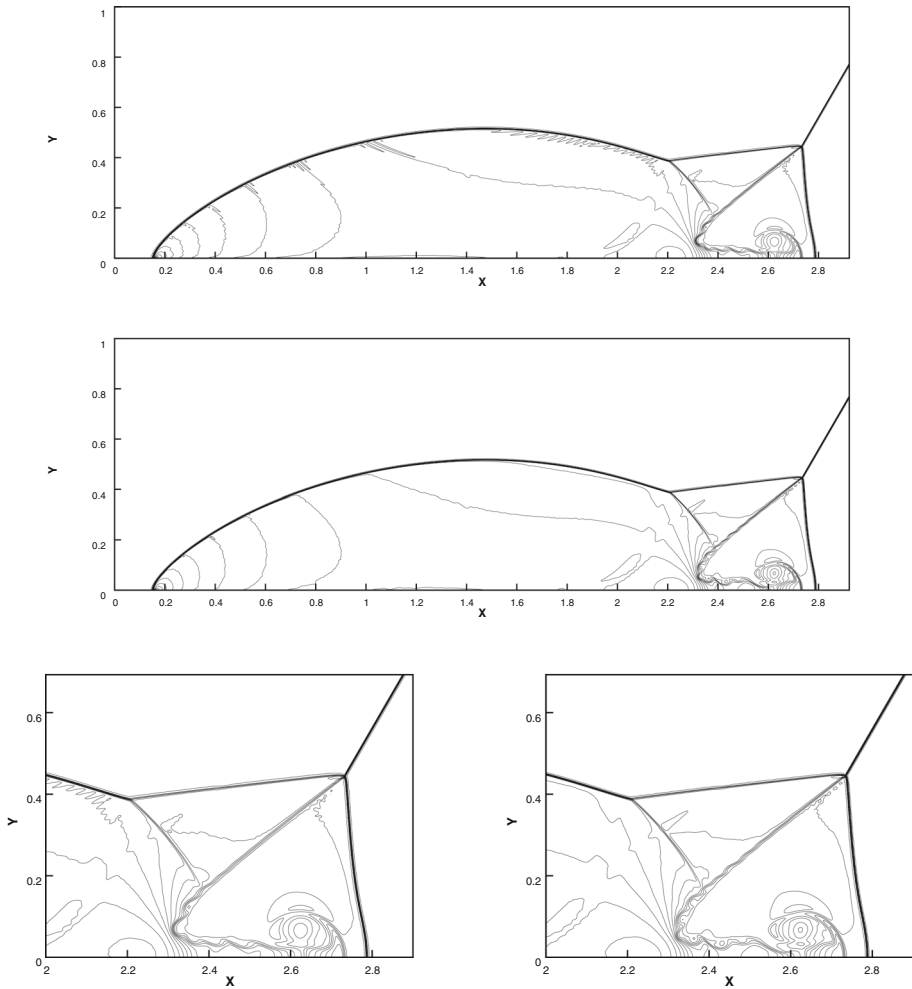


Fig. 7 Double Mach reflection problem. $T = 0.2$. 30 equally spaced density contours from 1.5 to 22.7. From top to bottom: the result of the classical WENO scheme; the result of the modified HWENO scheme; zoomed of the classical WENO and the modified HWENO schemes. Grid points: 1600×400

since the new cost of the modification procedure is offset by the fact that the new scheme is free of the flux limiter and can use a larger CFL number, while the modified HWENO scheme needs a little more computational cost than that of the classical WENO scheme [11], but the modified HWENO scheme is much more compact as only immediate neighbor information is used in the reconstructions with smaller numerical errors. Numerical experiments in the

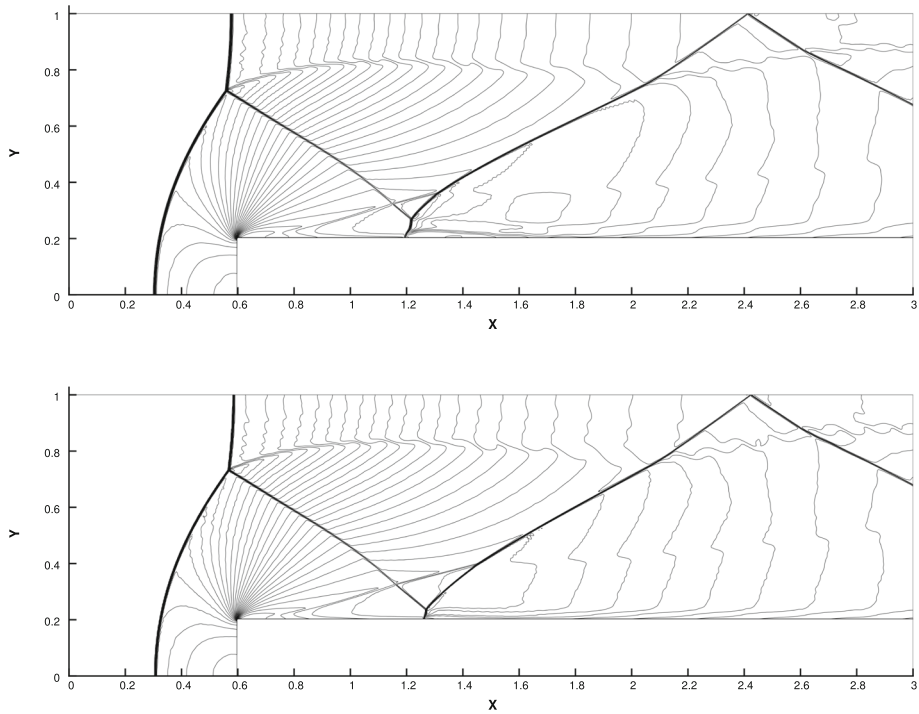


Fig. 8 Forward step problem. $T = 4$. 30 equally spaced density contours from 0.32 to 6.15. From top to bottom: the result of the the classical WENO scheme; the result of the modified HWENO scheme; Grid points: 960×320


paper show that the proposed modified fifth order finite difference HWENO scheme has better performances than the original finite difference HWENO scheme [15] and the classical fifth order finite difference WENO scheme [11].

References

1. Cai, X., Zhang, X., Qiu, J.: Positivity-preserving high order finite volume HWENO schemes for compressible Euler equations. *J. Sci. Comput.* **68**, 464–483 (2016)
2. Cai, X., Zhu, J., Qiu, J.: Hermite WENO schemes with strong stability preserving multi-step temporal discretization methods for conservation laws. *J. Comput. Math.* **35**, 19–40 (2017)
3. Castro, M., Costa, B., Don, W.S.: High order weighted essentially non-oscillatory WENO-Z schemes for hyperbolic conservation laws. *J. Comput. Phys.* **230**, 1766–1792 (2011)
4. Cockburn, B., Shu, C.-W.: TVB Runge-Kutta local projection discontinuous Galerkin finite element method for conservation laws II: general framework. *Math. Comput.* **52**, 411–435 (1989)
5. Dumbser, M., Balsara, D.S., Toro, E.F., Munz, C.D.: A unified framework for the construction of one-step finite volume and discontinuous Galerkin schemes on unstructured meshes. *J. Comput. Phys.* **227**, 8209–8253 (2008)
6. Harten, A.: High resolution schemes for hyperbolic conservation laws. *J. Comput. Phys.* **49**, 357–393 (1983)
7. Harten, A., Engquist, B., Osher, S., Chakravarthy, S.: Uniformly high order accurate essentially non-oscillatory schemes III. *J. Comput. Phys.* **71**, 231–323 (1987)
8. Harten, A., Osher, S.: Uniformly high-order accurate non-oscillatory schemes I. *SIAM J. Numer. Anal.* **24**, 279–309 (1987)

9. Hu, X.Y., Adams, N.A., Shu, C.-W.: Positivity-preserving method for high-order conservative schemes solving compressible Euler equations. *J. Comput. Phys.* **242**, 169–180 (2013)
10. Hu, C., Shu, C.-W.: Weighted essentially non-oscillatory schemes on triangular meshes. *J. Comput. Phys.* **150**, 97–127 (1999)
11. Jiang, G.-S., Shu, C.-W.: Efficient implementation of weighted ENO schemes. *J. Comput. Phys.* **126**, 202–228 (1996)
12. Levy, D., Puppo, G., Russo, G.: Central WENO schemes for hyperbolic systems of conservation laws. *Math. Model. Numer. Anal.* **33**, 547–571 (1999)
13. Li, G., Qiu, J.: Hybrid weighted essentially non-oscillatory schemes with different indicators. *J. Comput. Phys.* **229**, 8105–8129 (2010)
14. Liu, X.D., Osher, S., Chan, T.: Weighted essentially non-oscillatory schemes. *J. Comput. Phys.* **115**, 200–212 (1994)
15. Liu, H., Qiu, J.: Finite difference Hermite WENO schemes for conservation laws. *J. Sci. Comput.* **63**, 548–572 (2015)
16. Liu, H., Qiu, J.: Finite difference Hermite WENO schemes for conservation laws, II: an alternative approach. *J. Sci. Comput.* **66**, 598–624 (2016)
17. Luo, D., Huang, W., Qiu, J.: A hybrid LDG-HWENO scheme for KdV-type equations. *J. Comput. Phys.* **313**, 754–774 (2016)
18. Ma, Z., Wu, S.P.: HWENO schemes based on compact difference for hyperbolic conservation laws. *J. Sci. Comput.* **76**, 1301–1325 (2018)
19. Qiu, J., Shu, C.-W.: Hermite WENO schemes and their application as limiters for Runge–Kutta discontinuous Galerkin method: one-dimensional case. *J. Comput. Phys.* **193**, 115–135 (2004)
20. Qiu, J., Shu, C.-W.: Hermite WENO schemes and their application as limiters for Runge–Kutta discontinuous Galerkin method II: two dimensional case. *Comput. Fluid.* **34**, 642–663 (2005)
21. Shi, J., Hu, C., Shu, C.-W.: A technique of treating negative weights in WENO schemes. *J. Comput. Phys.* **175**, 108–127 (2002)
22. Shu, C.-W.: High order weighted essentially nonoscillatory schemes for convection dominated problems. *SIAM Rev.* **51**, 82–126 (2009)
23. Shu, C.-W., Osher, S.: Efficient implementation of essentially non-oscillatory shock capturing schemes. *J. Comput. Phys.* **77**, 439–471 (1988)
24. Shu, C.-W., Osher, S.: Efficient implementation of essentially non-oscillatory shock capturing schemes, II. *J. Comput. Phys.* **83**, 32–78 (1989)
25. Tao, Z., Li, F., Qiu, J.: High-order central Hermite WENO schemes on staggered meshes for hyperbolic conservation laws. *J. Comput. Phys.* **281**, 148–176 (2015)
26. Tao, Z., Li, F., Qiu, J.: High-order central Hermite WENO schemes: dimension-by-dimension moment-based reconstructions. *J. Comput. Phys.* **318**, 222–251 (2016)
27. Woodward, P., Colella, P.: The numerical simulation of two-dimensional fluid flow with strong shocks. *J. Comput. Phys.* **54**, 115–173 (1984)
28. Zahran, Y.H., Abdalla, A.H.: Seventh order Hermite WENO scheme for hyperbolic conservation laws. *Comput. Fluid.* **131**, 66–80 (2016)
29. Zhang, Y.-T., Shu, C.-W.: Third order WENO scheme on three dimensional tetrahedral meshes. *Commun. Comput. Phys.* **5**, 836–848 (2009)
30. Zhang, Y.-T., Shi, J., Shu, C.-W., Zhou, Y.: Numerical viscosity and resolution of high-order weighted essentially nonoscillatory schemes for compressible flows with high Reynolds numbers. *Phys. Rev. E* **68**, 046709 (2003)
31. Zhao, Z., Chen, Y., Qiu, J.: A hybrid Hermite WENO scheme for hyperbolic conservation laws. *J. Comput. Phys.* **405**, 109175 (2020)
32. Zhao, Z., Qiu, J.: A Hermite WENO scheme with artificial linear weights for hyperbolic conservation laws. *J. Comput. Phys.* **417**, 109583 (2020)
33. Zheng, F., Qiu, J.: Directly solving the Hamilton-Jacobi equations by Hermite WENO schemes. *J. Comput. Phys.* **307**, 423–445 (2016)
34. Zhu, J., Qiu, J.: A class of fourth order finite volume Hermite weighted essentially non-oscillatory schemes. *Sci. China Ser. A Math.* **51**, 1549–1560 (2008)
35. Zhu, J., Qiu, J.: A new fifth order finite difference WENO scheme for solving hyperbolic conservation laws. *J. Comput. Phys.* **318**, 110–121 (2016)

Affiliations

Zhuang Zhao¹ · Yong-Tao Zhang² · Jianxian Qiu³ 

✉ Jianxian Qiu
jxqiu@xmu.edu.cn

Zhuang Zhao
zzhao@stu.xmu.edu.cn

Yong-Tao Zhang
yztang10@nd.edu

¹ School of Mathematical Sciences, Xiamen University, Xiamen 361005, Fujian, People's Republic of China

² Department of Applied and Computational Mathematics and Statistics, University of Notre Dame, Notre Dame, IN 46556, USA

³ School of Mathematical Sciences and Fujian Provincial Key Laboratory of Mathematical Modeling and High-Performance Scientific Computing, Xiamen University, Xiamen 361005, Fujian, People's Republic of China